Pergamon

Cement and Concrete Research 30 (2000) 1401–1406

CEMENT AND CONCRETE RESEARCH

Effect of pore size distribution on drying shrinkage of alkali-activated slag concrete

Frank Collins[a,*], J.G. Sanjayan[b]

[a]*Maunsell Pty Ltd, Level 9, 161 Collins Street, Melbourne, Victoria 3000, Australia*
[b]*Department of Civil Engineering, Monash University, Clayton, Victoria 3168, Australia*

Received 20 September 1999; accepted 2 June 2000

Abstract

Higher drying shrinkage has been observed in alkali-activated slag concrete (AASC) than comparable ordinary Portland cement concrete (OPCC). However, the OPCC samples lost more moisture during the period of shrinkage measurements than the AASC samples. This is contradictory to the commonly accepted relationship between shrinkage and moisture loss. This paper provides an explanation for this phenomenon by studying the effect of pore size distribution on the drying shrinkage. The investigation showed that AAS pastes have a much higher proportion of pore sizes within the mesopore region than OPC pastes. Further, the radius of pores where the meniscus forms seems to be an important parameter in determining the magnitude of shrinkage, rather than the amount of moisture loss. This also supports the theory that the capillary tensile forces set up during drying is an important contributory factor for the drying shrinkage of concrete.

Keywords: Drying; Shrinkage; Pore size distribution; Alkali-activated cement; Granulated blast-furnace slag

1. Introduction

Alkali-activated slag binders based on 100% slag plus activator has been extensively reported in the literature; Talling and Brandstetr [1] and Roy [2] provide a comprehensive state of the art summary. Alkali-activated slag concrete (AASC) has been shown to have higher drying shrinkage than ordinary Portland cement concrete (OPCC) [3–8]. Kutti et al. [3] measured 12-month drying shrinkage of $NaOH + Na_2CO_3$-activated AASC that was 1.83 times the drying shrinkage of OPCC when exposed to 59% relative humidity (RH). Malolepszy and Deja [4] and Hakkinen [5] measured 1.6 times higher drying shrinkage of AAS mortars compared with OPC mortars. Collins and Sanjayan [7] measured 57% higher drying shrinkage of AASC than OPCC when subjected to 50% RH. The pore size distribution and the calcium silicate hydrate gel characteristics have a critical influence on the magnitude of drying shrinkage [9,10]. The precise nature of the microstructural model, which describes shrinkage behaviour, is subject to debate between three main models: the Powers model [11], Feldman–Sereda model [12], and Munich model [13]. Although the various models cite different mechanisms that contribute to shrinkage, namely disjoining pressures or water movement or water–solid interaction, or a combination of these, two common factors have a critical influence on shrinkage: the pore size distribution and the calcium silicate hydrate gel characteristics. Formation of a shrinkage-prone silica gel has been put forward as an explanation of this phenomenon [3,8,14].

Details of an experimental program carried out to study the influence of pore size distribution on drying shrinkage of AASC are reported in this paper. The pore size distribution was obtained from mercury intrusion porosimetry tests on AAS pastes. Initially, the tests were carried out on AAS concrete samples. However, the results from concrete samples were found to be highly variable due to the presence of randomly located aggregate particles. The porosimetry results on pastes were found to be very consistent and therefore all the pore distribution results reported in this paper are based on pastes.

* Corresponding author. Tel.: +61-3-9653-1234; fax: +61-3-9654-7117.
E-mail address: fgco@maunsell.com.au (F. Collins).

0008-8846/00/$ – see front matter
PII: S0008-8846(00)00327-6

2. Experimental program

2.1. Materials

The chemical composition and properties of the cementitious binders are summarised in Table 1. The binders used are ground granulated blast furnace slag (slag) and Portland cement (OPC). The term water/binder (w/b) ratio is used instead of water/cement ratio (w/c) to include both the binders mentioned above. The slag is supplied with preblended gypsum containing 2% SO_3. The activators and adjuncts utilised were powdered sodium metasilicate and hydrated lime. The method of use in concrete has been outlined earlier by Collins and Sanjayan [7].

The coarse aggregate consisted of 14-mm maximum size basalt with a specific gravity of 2.95 and 24-h water absorption of 1.2%. The fine aggregate consisted of river sand with a specific gravity of 2.65, 24-h water absorption of 0.5%, and a fineness modulus of 2.19.

The concrete mixture proportions for OPC concrete (OPCC) and AAS concrete (AASC) are summarized in Table 2. The materials used for concrete making, the method of preparing concrete mixes in the laboratory, and the tests for fresh and mechanical concrete properties reported in this paper were in accordance with the Australian Standard AS1012, except for the type of curing. Shrinkage prisms were made of dimensions 75 × 75 × 285 mm and following demoulding after 24 h, a triplicate set of samples were exposed to 23°C and 50% RH.

2.2. Testing of pastes by mercury intrusion porosimetry

Mixing of OPC and AAS pastes was conducted in a 20-l stainless steel mixing bowl. Mixing was by machine mixing at 98 revolutions per minute in a Kenwood KNM20 planetary mixer. For OPC paste, following weighing of the correct quantities of binder and water, the sequence of mixing consisted of 2 min mixing followed by 2 min of rest, followed by further mixing for 2 min. The slag and the sodium silicate activator were preblended in the dry form for 2 min. The mixing water was then added. The hydrated lime was added as a 1:3 hydrated lime:water slurry. The mixing procedure was the same as for the OPC paste. The fluid pastes were poured into cylindrical moulds, which had internal dimensions of 63-mm diameter × 98-mm length. The w/b*** of OPC and AAS pastes was 0.5. Following demoulding at 1 day, samples from each paste type were exposed to 23°C and 50% RH for 3, 7, 28, and 56 days. At the required time of test, the samples were crushed to a size adequate to pass a 2.36-mm sieve.

The pore size distribution was determined using a Micromeritics Autopore III 9429 porosimeter which was capable of pressures from 0 to 414 MPa (60 000 psi). A hydraulic pump generates the pressure and a contact sensor measures the mercury volume. All operations are automated by microprocessor and are conducted within a fully enclosed pressure chamber. The assumed surface tension of the triple-distilled mercury was 0.484 N/m at 25°C (ASTM D 4404-84 1992). The density of the mercury was 13.546 g/ml and the assumed contact angle was 140°.

Table 1
Properties of cementitious materials

Constituent/property	Slag	OPC
SiO_2 (%)	35.04	19.9
Al_2O_3 (%)	13.91	4.62
Fe_2O_3 (%)	0.29	3.97
MgO (%)	6.13	1.73
CaO (%)	39.43	–
Na_2O (%)	0.34	–
TiO_2 (%)	0.42	–
K_2O (%)	0.39	0.57
P_2O_5 (%)	<0.1	–
MnO (%)	0.43	–
Total sulphur as SO_3 (%)	2.43	2.56
Sulphide sulphur as S^{2-}	0.44	–
Cl (ppm)	80	–
Fineness (m^2/kg)	460	342
Loss on ignition (%)	1.45	2.9
Time to initial set (h)	N/A	2.0
Strength of 75 × 75 × 75 mm mortar cubes (MPa)	N/A	32.7
3 Days		42.0
7 Days		54.1
28 Days		

Table 2
Summary of concrete mixture proportions (kg/m^3)

Constituents	OPCC	AASC[a]
OPC	360	–
Slag	–	360
Free water[b]	180	180
w/b	0.5	0.5
Fine aggregate	830	830
Coarse aggregate, 14 mm	1130	1130
Air content (%)	0.5	1.2

[a] Slag activated by powdered sodium silicate and lime slurry.
[b] Adjustments made for water in aggregates (to saturated surface dry

3. Drying shrinkage and weight loss

Results of drying shrinkage are summarized in Fig. 1. AASC shows considerably higher rate of drying shrinkage as compared with OPCC. The weight change of the shrinkage prisms due to egress of moisture from the sample, expressed as percent weight change of the total specimen weight is shown in Fig. 2. OPCC generally shows greater weight loss during drying than AASC.

The differences in weight loss between OPCC and AASC tend to converge towards 365 days. Kutti [3] and Malalepszy and Deja [4] also measured higher weight loss in OPCC than AASC. OPCC loses more weight of water during drying than AASC yet shows significantly lower

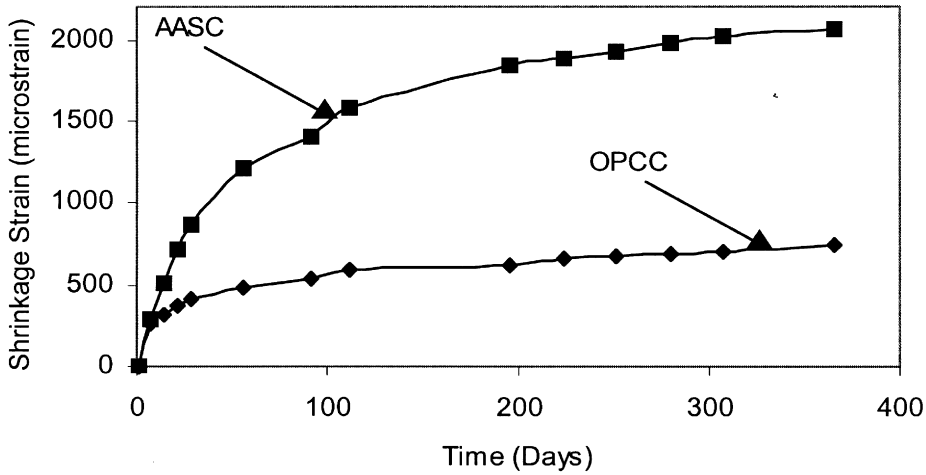

Fig. 1. Drying shrinkage of OPCC and AASC, esposed from day 1 onwards to 50% RH and 23°C, w/h = 0.5.

magnitude of shrinkage. Therefore, the it must be concluded that the mechanism of high drying shrinkage of AASC is not entirely due to the quantity of weight loss of water from the concrete. Previous studies by Wittmann [9] and Young [10] show that the pore size distribution and the calcium silicate hydrate gel characteristics have a critical influence on the magnitude of drying shrinkage.

4. Influence of pore size distribution on drying shrinkage

Pore sizes can be classified according to the International Union of Pure and Applied Chemistry (IUPAC) system [15] as described in Table 3.

The capillary pores comprise both the mesopores and macropores and constitute the water filled space existing between original cement grains, whereas the micropores constitute part of the calcium silicate hydrate gel component. Shrinkage under practical conditions depends on loss of water from the mesopores and also the size of the macropores, which determines how easily water may be lost from the mesopores [10].

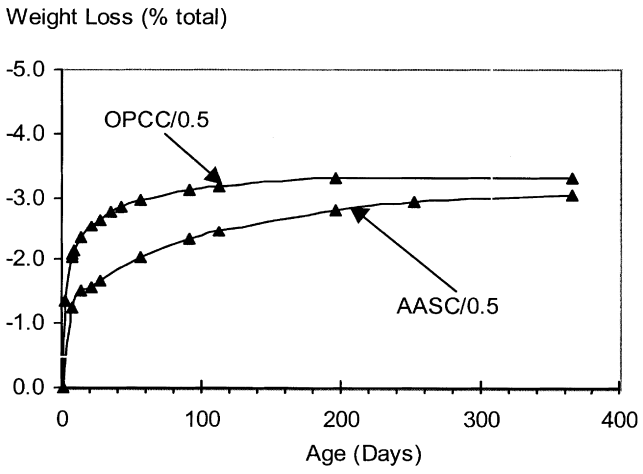

Fig. 2. Weight loss of shrinkage prisms when exposed from day 1 onwards.

The pore size distribution of slag–OPC blended cements becomes finer with increasing slag content [16,17]. In the case of alkali-activated slag, the proportion of pores in the micropore size range tend to be higher than OPC [5,18–22]. The number of pores within the capillary range is lower than OPC [21–23]. Following fog room curing, Shi [24] found OPC to have a continuous pore size distribution within the 5- to 1200-nm pore sizes whereas sodium-silicate-activated slag contained pores either in the sizes less than 10 nm or greater than 200 nm.

Fig. 3 shows the envelope of cumulative pore size distribution for OPC paste (OPCP) and AAS paste (AASP) which were measured at 3, 7, 28, and 56 days. The envelopes show AASP has a finer pore size distribution than OPCP.

Analysis of the incremental pore size distribution data shows that AASP has a much higher proportion of pore sizes within the mesopore limits than OPCP, as shown in Table 4. The proportion of pores within the mesopore classification ranges from 74.0% to 82.0% for AASP compared with 24.7–36.4% for OPCP. The higher total

Table 3
IUPAC pore size classification

Pore description	Radius (nm)
Micropores	<1.25
Mesopores	1.25–25
Macropores	25–5000
Entrained air voids, entrapped air voids, preexisting microcracks	5000–50 000

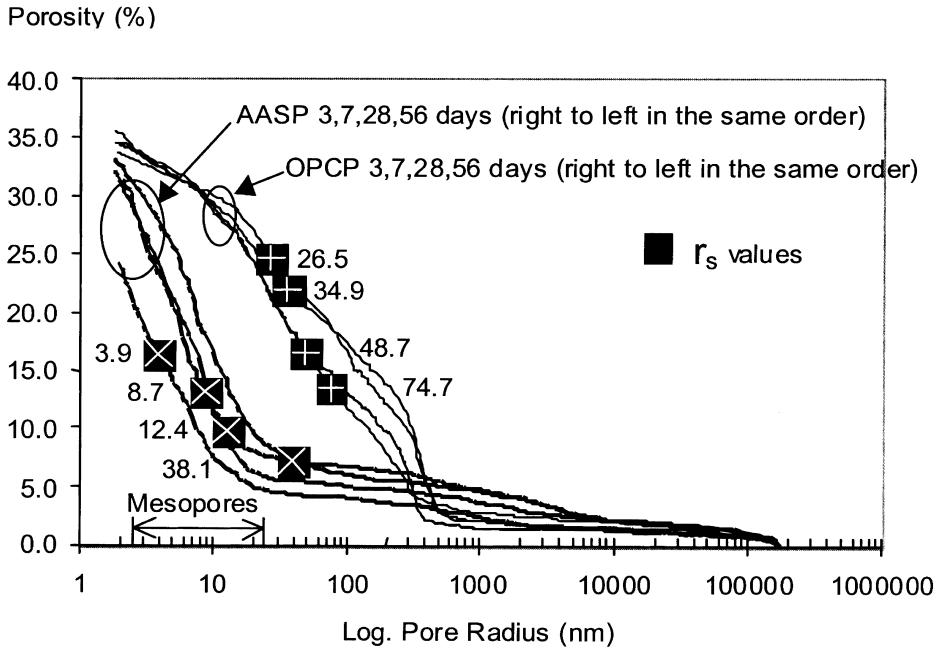

Fig. 3. Cumulative pore size distribution of OPCP and AASP at 3, 7, 28, and 56 days.

volume of mesopores in AASP could explain the higher magnitude of drying shrinkage of AASC.

5. Effect of capillary tensile forces on drying shrinkage

Shimomura and Maekawa [25,26] and Shimomura [27] proposed a micromechanical model to describe drying shrinkage behaviour that was based on pore size distribution and thermodynamic behaviour of water in the pores. Part of the model involved computation of a parameter r_s, which is defined as the radius of the pores where the meniscus forms; i.e., the pores whose radii are smaller than r_s are assumed to be filled with liquid water while pores larger than this are dry. As the drying progresses, the parameter r_s would decrease. It was hypothesized by the researchers [25–27] that the smaller the parameter r_s the larger the capillary tensile forces set up at the meniscus (the interface between water and air), hence higher the resulting shrinkage.

Weight-loss data for AASC and OPCC, which was discussed above, was used to determine the volume of water that was dried from the paste. Compensation was made to

Table 4
Pore size proportions with IUPAC classifications for AASP and OPCP

	% Mesopores		% Macropores		% Voids/microcracks	
Age (days)	AASP	OPCP	AASP	OPCP	AASP	OPCP
3	74.0	36.4	16.6	56.7	9.4	6.9
7	76.0	35.2	14.9	59.6	9.1	5.2
28	82.0	32.7	10.4	62.2	7.6	5.1
56	81.3	24.7	12.5	69	6.2	6.3

Table 5
Computaion of r_s and values of measured shrinkage

	OPC				AAS			
Age (days)	3	7	28	56	3	7	28	56
Drying shrinkage (exposed) ε_{ex}	94	255	413	488	159	293	865	1204
Shrinkage (sealed) ε_{se}	3	43	184	241	19	59	205	299
$\varepsilon_{ex} - \varepsilon_{se}$	91	212	229	247	140	234	660	905
% Moisture loss from prisms	1.61	2.03	2.65	2.96	0.90	1.23	1.67	2.03
Volume of water dried for paste, V_d (%)	13.4	16.9	22.1	24.7	7.4	10.1	13.7	16.6
Total porosity % (from porosimetry on pastes)	34.7	34.4	35.6	33.6	33.2	32.2	31.4	24.3
r_s (from PSD using volume water dried), nm	74.7	48.7	34.9	26.4	38.1	12.4	8.7	3.9

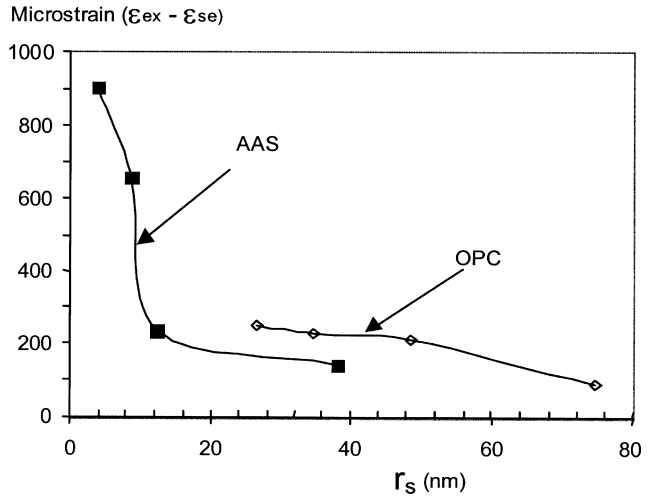

Fig. 4. Drying shrinkage (excluding autogenous shrinkage) versus r_s for AAS and OPC; w/b = 0.5.

account for the relative proportions and densities of the concrete constituents. The cumulative pore size distribution (PSD) curves were then used to calculate r_s. Values of r_s are shown in Fig. 3 and Table 5.

In the case of activated slag, Fig. 3 shows values of r_s are within the 3.9–38.1 nm range, whereas OPCP values of r_s are larger than the mesopores. There are significantly fewer pores within the macropore region for AASP and hence drying of water affects the pores within the mesopore region more quickly (per amount of water weight loss) than OPCP. This would explain that the weight loss during drying of AASC is less than OPCC whereas the magnitude of drying shrinkage is significantly higher.

Fig. 4 shows measured shrinkage strain versus r_s for the two binder types. When r_s becomes less than 16 nm, the rate of shrinkage rapidly increases. Significant drying of mesopore water takes place in the case of activated slag and this would explain the difference in behaviour between the binder types.

6. Conclusions

1. Investigation of drying shrinkage of AASC shows the magnitude of drying shrinkage is greater than OPCC for equivalent concretes.
2. The weight loss during drying is less for AASC than OPCC, although the magnitude of shrinkage strain is greater.
3. The pore size distribution shows up to 82% pores in the mesopore range for AASP compared with 36.4% for OPCP. Analysis of weight loss data indicates that drying of water from mesopores occurs with AASP compared with OPCP, which shows none, and this may be the reason for higher drying shrinkage of AASP.
4. Although the AAS samples lost less moisture than OPC samples, the radius of pore where the meniscus forms is smaller for the AAS than OPC pastes. The results support the theory that capillary tensile forces set up during drying is a very significant factor for the drying shrinkage of AAS.

Acknowledgments

The financial support for this project is jointly provided by Independent Cement and Lime Pty, Blue Circle Southern Cement and Australian Steel Mill Services. The authors thank the sponsors especially Alan Dow, Tom Wauer, Katherine Turner, Wayne James, Paul Ratcliff, John Ashby, and Dr. Ihor Hinczak for the guidance and support. The enthusiastic participation of final-year students Dennis Kueh, Soon Keat Lim, and Eric Tan in this project is very much appreciated. The efforts and assistance with the laboratory work provided by Jeff Doddrell, Roger Doulis, and Peter Dunbar are also gratefully acknowledged.

The work presented in this paper was carried out as part of Frank Collins' PhD thesis at the Department of Civil Engineering, Monash University.

References

[1] B. Talling, J. Brandstetr, Present state and future of alkali-activated slag concretes, Proc. 3rd Int. Conf. on Fly Ash, Slag, and Natural Pozzolans in Concrete, Trondheim, Norway, ACI SP-114 2, American Concrete Institute, 1989, pp. 1519–1546.
[2] D.M. Roy, Alkali-activated cements: opportunities and challenges, Cem Concr Res 29 (2) (1999) 249–254.
[3] T. Kutti, L. Berntsson, S. Chandra, Shrinkage of cements with high content of blast-furnace slag, . Proc. 4th CANMET/ACI Int. Conf. on Fly Ash, Slag, and Natural Pozzolans in Concrete, Istanbul, Turkey, American Concrete Institute, 1992, pp. 615–625 Supplementary papers.
[4] J. Malolepszy, J. Deja, The influence of curing conditions on the mechanical properties of alkali activated slag binders, Silic Ind 11 (12) (1988) 179–186.
[5] T. Hakkinen, The microstructure of high strength blast furnace slag concrete, Nord Concr Res 11 (1992) 67–82.
[6] E. Douglas, A. Bilodeau, V.M. Malhotra, Properties and durability of alkali-activated slag concrete, ACI Mater J 89 (5) (1992) 509–516.
[7] F. Collins, J.G. Sanjayan, Cem Concr Res 29 (3) (1999) 455–458.
[8] H. Kukko, R. Mannonen, Chemical and mechanical properties of alkali-activated blast furnace slag (F-concrete), Nord Concr Res 1 (1982) 16.1–16.16.
[9] F.H. Wittmann, Creep and shrinkage mechanisms, in: Z.P. Bazant, F.H. Wittmann (Eds.), Creep and Shrinkage in Concrete Structures, Wiley, Chichester, 1982, pp. 129–161.
[10] J.F. Young, Physical mechanisms and their mathematical descriptions, in: Z.P. Bazant (Ed.), Mathematical Modelling of Creep and Shrinkage of Concrete, Wiley, Chichester, 1988, pp. 63–98.
[11] T.C. Powers, The thermodynamics of volume change and creep, Mater Constr 1 (6) (1968) 487–507.
[12] R.F. Feldman, P.J. Sereda, The model for hydrated Portland cement paste as deduced from sorption-length change and mechanical properties, Mat and Constr 1 (1968) 509–520.

[13] F.H. Wittmann, Interaction of hardened cement paste and water, J Am Ceram Soc 56 (8) (1973) 409–415.
[14] S.D. Wang, Alkaline activation of slag, PhD dissertation, Imperial College of Science, Technology and Medicine, University of London, 1995.
[15] IUPAC, Manual of symbols and terminology, appendix 2, part 1, Colloid and Surface Chemistry, J Pure Appl Chem 31 (1972) 578.
[16] O.E. Gjorv, O. Vennesland, Diffusion of chloride ions from seawater into concrete, Cem Concr Res 9 (2) (1979) 229–238.
[17] P.K. Mehta, Pozzolanic and cementitious by-products as mineral admixtures for concrete — a critical review, in: V.M. Malhotra (Ed.), Proc. First CANMET/ACI International Conference on Fly Ash, Slag, Silica Fume and Other Natural Pozzolans in Concrete, Montebello, Canada, ACI SP-79 vol. 1, American Concrete Institute, 1983, pp. 1–46.
[18] V. Glukhovsky, Y. Zaitsev, V. Pakhomov, Slag–alkaline cements and concretes — structure, properties, technological and economical aspects of the use, Silic Ind 10 (1983) 197–200.
[19] C. Shi, R.L. Day, X. Wu, M. Tang, Comparison of the microstructure and performance of alkali-slag and Portland cement pastes, Proc. 9th International Congress on the Chemistry of Cement, New Delhi, India vol. 3, 1992, pp. 298–304.
[20] T. Hakkinen, The influence of slag content on the microstructure, permeability and mechanical properties of concrete: Part 2. Technical properties and theoretical examinations, Cem Concr Res 23 (3) (1993) 518–530.
[21] J. Malolepszy, J. Deja, Effect of heavy metals immobilization on the properties of alkali activated slag mortars, in: V.M. Malhotra (Ed.), Proc. 5th CANMET/ACI International Conference on Fly Ash, Silica Fume, Slag, and Natural Pozzolans in Concrete, Milwaukee, USA, ACI SP-153 vol. 2, American Concrete Institute, 1995, pp. 1087–1102.
[22] C. Shi, C. Day, Alkali-slag cements for the immobilisation of radioactive wastes, in: M. Gilliam, C.C. Wiles (Eds.), Stabilisation and Solidification of Hazardous, Radioactive and Mixed Wastes, ASTM STP-1240 vol. 3, American Society of Testing and Materials, 1996, pp. 163–173.
[23] J. Deja, J. Malolepszy, Long term resistance of alkali-activated slag mortars to chloride solution, Proc. Third CANMET/ACI Int. Conf. on Durability of Concrete, Nice, France, American Concrete Institute, 1994, pp. 657–671 Supplementary papers.
[24] C. Shi, Strength, pore structure and permeability of alkali-activated slag mortars, Cem Concr Res 26 (12) (1996) 1789–1799.
[25] T. Shimomura, K. Maekawa, Micromechanical model for drying shrinkage of concrete based on the distribution function of porosity, in: Z.P. Bazant, I. Carol (Eds.), Proc. 5th International RILEM Symposium on Creep and Shrinkage of Concrete, Barcelona, Spain, E & FN Spon, London, 1993, pp. 133–139.
[26] T. Shimomura, K. Maekawa, Analysis of the drying shrinkage behaviour of concrete based on the micropore structure of concrete using a micromechanical model, Mag Concr Res 49 (181) (1997) 303–322.
[27] T. Shimomura, Modelling of initial defect of concrete due to drying shrinkage, Proc. CONSEC '98 Concrete Under Severe Conditions, Norway vol. 3, 1998, pp. 2071–2083.